Title
Order, Chaos and Nuclear Dynamics

Authors
Blocki, J.
Shi, J.-J.
Swiatecki, W.J.

Publication Date
1991-11-01

LBL-31563
Preprint

Lawrence Berkeley Laboratory
UNIVERSITY OF CALIFORNIA

Submitted to Nuclear Physics A

Order, Chaos and Nuclear Dynamics

J. Blocki, J.-J. Shi, and W.J. Swiatecki

November 1991

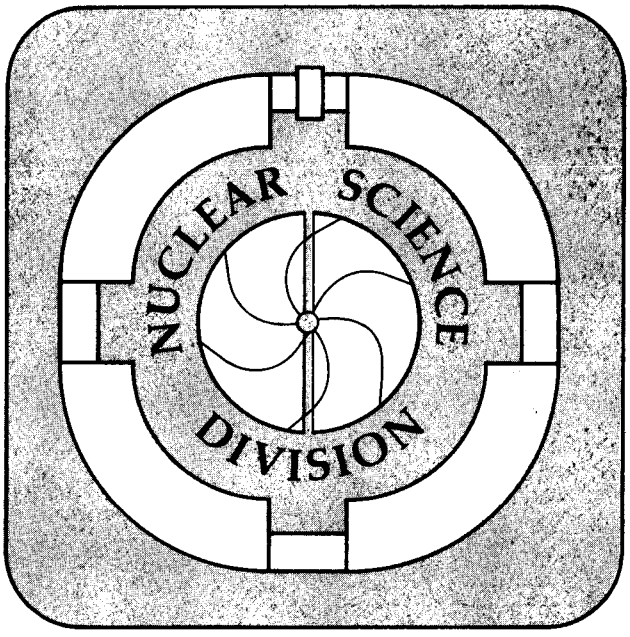

Prepared for the U.S. Department of Energy under Contract Number DE-AC03-76SF00098

DISCLAIMER

DISCLAIMER

LBL-31563

Order, Chaos and Nuclear Dynamics*

J. Blocki,† J.-J. Shi‡ and W.J. Swiatecki

Nuclear Science Division
Lawrence Berkeley Laboratory
University of California
Berkeley, California 94720

July 1987, revised November 1991

†Permanent address: Institute for Nuclear Studies, Swierk, Poland
‡Permanent address: Institute of Atomic Energy, P.O. Box 275(18), Beijing, China

*This work was supported by the Director, Office of Energy Research, Division of Nuclear Physics of the Office of High Energy and Nuclear Physics of the U.S. Department of Energy under Contract No. DE-AC03-76SF00098.

Order, Chaos and Nuclear Dynamics

J. Blocki,† J.-J. Shi‡ and W.J. Swiatecki

Nuclear Science Division
Lawrence Berkeley Laboratory
University of California
Berkeley, California 94720

Abstract

The relation between the order-to-chaos transition in the dynamics of independent classical particles in a container, and the transition from an elastic to a dissipative response of the container to shape changes, is studied by means of computer simulations. The validity of the wall formula for energy dissipation is confirmed in the case of containers whose surfaces are rippled according to Legendre Polynomials P_3, P_4, P_5, P_6, in which case the particle trajectories are largely chaotic, as revealed by Poincaré sections in phase space. The opposite limit of an elastic response is illustrated by means of spheroidal containers of various eccentricities, for which the particle trajectories are integrable and the phase space is foliated by tori. Fission-like deformations are also considered, for which the response of the container changes from elastic to dissipative with increasing deformation. Idealized giant-dipole oscillations of the gas are studied for spherical as well as deformed containers. A generalization of the wall formula valid for long times (i.e., for arbitrarily large excitations of the gas) is constructed. The principal lesson of these studies is that a gas of independent particles in a time-dependent container does not behave at all like a gas.

†Permanent address: Institute for Nuclear Studies, Swierk, Poland
‡Permanent address: Institute of Atomic Energy, P.O. Box 275(18), Beijing, China

1. Introduction

The study of the transition from order to chaos in dynamical systems is a major theme of contemporary science (Refs. 1-5). The full realization of the relevance of such studies to nuclear problems is relatively recent. It concerns two major aspects: on the one hand the statistical theory of nuclear level densities and, on the other, the nature of collective nuclear dynamics (Refs. 5-23). The latter is the motivation for the present paper.

In the past few years it has become apparent that the character of collective nuclear dynamics is intimately related to the nature of the nucleonic motions inside the nuclear mean-field potential well. If the nucleonic motions are ordered, the nucleus as a whole is expected to behave like an elastic solid, whereas for chaotic nucleonic motions the nucleus should behave like a very viscous fluid (Refs. 20-22). In the intermediate regime a visco-elastic behaviour is expected (Ref. 24). It follows that in order to understand collective processes such as nuclear fission or the dynamical evolution of two colliding nuclei, it is essential to understand under what conditions nucleonic motions will be ordered or chaotic. It is also necessary to study the transition from one type of behaviour to the other, a transition that may be induced by changes of the nuclear shape or other variables, such as the nuclear temperature.

Nuclear collective dynamics has been studied for a long time using various analytical approximations, as well as extensive computer modeling based on numerical solutions of the time-dependent Hartree-Fock or related equations (Ref. 25). By and large, these methods were developed before the relevance to nuclear dynamics of the order to chaos transition was fully appreciated. Another approach to this problem, the 'Chaotic Regime Dynamics,' was introduced several years ago (Ref. 6). It is a more primitive statistical theory which, however, was built directly on the assumption of chaotic nucleonic motions. A striking feature of this type of dynamics is that the nuclear shape changes are predicted to be often dominated by a new kind of viscosity, the 'one-body' dissipation. It was also realized quite early that in the case of ordered rather than chaotic motions, the response of the nucleus would probably be more like that of an

elastic solid. The resulting hypothesis of a parallelism between order or chaos on the one hand, and elastic or dissipative response on the other, was originally based on a limited number of studies of an idealized system consisting of a gas of non-interacting point particles in a time-dependent container, i.e., an extreme example of a 'Knudsen' gas (Ref. 26).

Most of these studies were at the classical level, with only a few cases backed up by a numerical solution of the corresponding time-dependent Schroedinger equation. A significant development in this field was the introduction into the nuclear context of the method of Poincaré sections in phase space, a powerful diagnostic tool for studying the transition from order to chaos in dynamical systems. Using this technique, the Grenoble school in particular has been investigating the order to chaos transition for point nucleons moving in sharp or diffuse spheroidal potential wells meant to approximate the nuclear mean field (Refs. 27-30). ✓

The present paper is a contribution to such idealized studies of nuclear dynamics. It extends the early numerical investigations of the elastic or dissipative response of a gas of particles in a time-dependent container, and juxtaposes them with Poincaré sections that serve to illuminate the transition from order to chaos in the particle trajectories. As with many numerical studies of this type, the particle motions are treated classically. (A perspicuous quantal analogue of a Poincaré section remains to be developed.) It follows that the results of the present paper are still far from providing a quantitative basis for understanding the relation of collective dynamics to the order to chaos transition in a relatively small quantal system, such as a nucleus. There are, nevertheless, indications that some of the qualitative results may survive the quantization of the particle motions. (In special cases even a quantitative correspondence is to be expected, see Ref. 20). In any event, the classical studies should serve as a useful guide and as a limiting test case for current quantal investigations of the same problem.

In Section 2 we present a number of numerical studies of a gas of point particles bouncing about in an oscillating, axially symmetric container. The total energy of the particles is followed as a function of time, and this serves to illustrate the elastic response of the gas for near-spheroidal containers (when the particle motions are integrable), and a dissipative response for more

irregularly shaped containers, described by ripples proportional to Legendre polynomials P_3, P_4, P_5, and P_6. An aperiodic, fission-like time dependence of an originally spherical container is also studied. In Section 3 the sloshing of the above gas of independent particles in a fixed container, mimicking the nuclear giant dipole oscillation, is examined.

Section 4 is devoted to a systematic illustration of the Poincaré sections for particles in variously deformed (but static) containers. The six types of shapes examined correspond to various degrees of spheroidal and of Legendre-polynomial deformations P_2 through P_6.

Section 5 summarizes the results and the Appendix gives the derivation of a dissipation formula valid when the relative excitation of the gas is no longer small.

2. Classical (Knudsen) gas in a time-dependent container.

Figures 1–4 are extensions of studies reported in Ref. 6. A hard-walled container of fixed volume $\frac{4}{3}\pi R_o^3$ (a three-dimensional 'billiard') is filled with a gas of several thousand non-interacting point particles, whose positions within the container are chosen at random and whose velocity vectors are also chosen at random to lie within a Fermi sphere of radius v in velocity space. The container is now made to undergo harmonic oscillations with assigned multipolarity, amplitude and frequency. The relative change in the energy of the gas $(E-E_o)/E_o$, is followed in time for a number of oscillations. (This is done by following numerically each independent particle's trajectory inside the oscillating container and adding up all the particles' instantaneous energies.)

Figure 1 shows the relative energy change for five complete cycles in the case of an axially symmetric container oscillating around the spherical configuration according to surface deformations proportional to Legendre polynomials P_n, with n = 2, 3, 4, 5, or 6. The radius vector $R(\theta,t)$ specifying the surface at time t was taken as

$$R(\theta,t) = R_o\left\{1 + \left[\alpha_n P_n(\cos\theta) + \alpha_1 P_1(\cos\theta)\right]\cos\omega t\right\}/\lambda(t) \qquad (1)$$

where $\lambda(t)$ is a normalization factor ensuring volume conservation and α_1 ensures fixity of the center of mass (Ref. 31).

At the beginning of the oscillation, at t = 0, the maximum displacement of the P_n deformation is α_n. These maximum amplitudes were taken to be given by $\sqrt{(2n+1)/5}\ \alpha$, which means that, for a given (small) α, the root mean square deviation of the surface from a sphere is the same for all multipolarities n. At t = 0 the surface velocity is zero, so the motion is started relatively gently, avoiding as far as possible transients associated with the initiation of the oscillations. The most rapidly moving part of the container's surface is the tip specified by $\theta = 0$ or π and its speed is a maximum when $\sin \omega t = 1$. This maximum speed is $\sqrt{(2n+1)/5}\ \alpha\omega R_o$, equal to $\alpha\omega R_o$ for n = 2. We shall define the adiabaticity index η as the ratio of $\alpha\omega R_o$ to the maximum particle speed v, viz.:

$$\eta = \alpha\omega R_o / v \ . \tag{2}$$

The smaller η, the more nearly adiabatic are the shape changes in relation to representative particle velocities. We shall also define a frequency index ν as the ratio of the time for a particle with velocity v to bounce back and forth across the standard diameter $2\ R_o$, to the oscillation period $T = 2\pi/\omega$, viz.:

$$\nu = \frac{4\ R_o}{v} \Big/ \frac{2\pi}{\omega} = \frac{2}{\pi}\frac{\eta}{\alpha} \ . \tag{3}$$

Note that if α is sufficiently small, the oscillation may be adiabatic in the sense that η is small, but the oscillation frequency may nevertheless be large compared to typical particle transit times.

All the curves in Fig. 1 refer to rather adiabatic oscillations with $\eta = 0.04$ and an amplitude corresponding to $\alpha = 0.02$. The frequency index is thus $\nu = 0.1273$. Except for the case n = 2, all the curves show a monotonic increase of the excitation energy and agree fairly well with the so-called wall formula for one-body dissipation. According to this formula the rate of energy flow from the walls of the container to the particles is given by

$$\frac{dE}{dt} = \rho \bar{v} \oint \dot{n}^2 \, d\sigma \ , \tag{4}$$

where ρ is the mass density of the gas, $\bar{v}$ the mean particle speed (equal to $\frac{3}{4}v$ in our case), $\dot{n}$ is the normal velocity of a surface element $d\sigma$, and the integral is over the surface of the container. [The physical effect behind the wall formula is the slight excess in the speeding up of particles bouncing off an approaching surface element over the slowing down when the surface element is receding (Ref. 6).]

Integrating Eq. 4 up to time t one readily verifies that (for small α) the relative energy increase of the gas should be given by

$$\Delta = (E - E_o)/E_o = \frac{3}{4}\alpha\eta\left(\omega t - \frac{1}{2}\sin 2\omega t\right) . \qquad (5)$$

This is a monotonic increase consisting of a part linear in t modulated by a periodic ripple. The linear part may be written as (3/4) $\alpha\eta 2\pi N$, where N is the number of periods. This linear trend is indicated by the dashed line in Fig. 1. After five complete oscillations the relative energy increase should be (0.75) (0.2) (0.04) $2\pi(5) = 0.1885$ in our case. The actual wall formula prediction, including the modulations, would be essentially indistinguishable from the numerical result for n = 5 in Fig. 1(b).

The wall formula is based on the assumption of chaotic particle motions and the fair agreement with the curves for n = 3, 4, 5, 6 suggests that this assumption is satisfied to a substantial degree. By contrast, the case n = 2 shows a drastic deviation. As discussed in Ref. 6, this is associated with the fact that, for small amplitudes, a P_2 distortion represents approximately a spheroidal deformation, which is known to correspond to an integrable situation, with ordered rather than chaotic particle motions inside the container. The decisive effect of integrability is confirmed in Fig. 2a, which displays $(E-E_o)/E_o$ for the case of a spheroidal container whose surface is described by

$$\frac{x^2}{a(t)^2} + \frac{y^2}{a(t)^2} + \frac{z^2}{c(t)^2} = 1 , \qquad (6)$$

where

$$c(t) = R_o\,(1 + \alpha \cos \omega t) \tag{7}$$

$$a(t) = R_o\,(1 + \alpha \cos \omega t)^{-1/2} \tag{8}$$

so that $a^2c = R_o^3$ and volume is conserved. The three curves in Fig. 2a correspond to $\eta = 0.03$, 0.02, and 0.01 (i.e., $\nu = 0.0955$, 0.0637 and 0.0318). An extrapolation to $\eta = 0$ indicates that for vanishingly slow oscillations the gas would respond to deformations like an elastic solid rather than a normal gas. (A normal gas, if deformed slowly at constant volume, would show no change in its energy.) The modulus of elasticity of the spheroidal system against spheroidal (quadrupole) stretchings may be deduced by writing

$$\Delta E = E - E_o = \frac{1}{2} K\alpha^2 \tag{9}$$

and noting from Fig. 2a that a change from $\alpha = 0.2$ (at $t = 0$) to $\alpha = -0.2$ (at $\omega t = \pi$) increased the energy by about $0.03\ E_o$. Hence

$$K \approx 2(0.03\ E_o)/(0.4)^2 \approx (3/8)\ E_o\ . \tag{10}$$

We note in passing that if the gas were confined by a parallel-sided box, its modulus of elasticity against a quadrupole stretching parallel to one of the edges would be $2\ E_o$ (Ref. 20).

Figure 2a also shows that for a small but finitite speed of oscillation the response of the gas exhibits a small monotonically increasing dissipative background on top of which are superimposed the reversible elastic bumps of about 3%. The background increases monotonically with the adiabaticity index η and may reflect the fact that for any given η there are always *some* particles near the center of the Fermi sphere in velocity space for which the oscillations of the container are highly non-adiabatic. The effect of non-adiabaticity is illustrated in Fig. 2b, where η has been increased to 0.1, 0.2 and 0.3 (i.e., $\nu = 0.3183$, 0.6366 and 0.9549). The plot of $(E - E_o)/E_o$ is now against time expressed in units of R_o/v. Thus, after 60 of these time units, the system has undergone 4.77, 9.55 and 14.32 cycles for $\eta = 0.1$, 0.2 and 0.3, respectively. The

first case can again be interpreted as an approximately elastic response of about 3% on top of a background which is now comparable, at about 4%. For $\eta = 0.2$ the background is now some 8–10% and the bumps are smaller and less regular. For $\eta = 0.3$, where the frequency index is close to 1, the excitation curve has changed character. There is a dominating, monotonically increasing component, which reaches 40% at the end of 14 cycles.

Figure 3a illustrates the effect of a higher η (= 0.1414) and a higher ν (= 0.900) in the case of a P_2 oscillation. The amplitude is only 0.1 in this case, so the oscillation is to a fair approximation spheroidal. The excitation curve appears to level out at about 5.5%, approximately in line with the trend of the two lower curves in Fig. 2b. The absence of regular elastic bumps might be associated with the higher value of the frequency index ν in this case.

Figure 3b illustrates the effect of increasing ν for a more nearly chaotic system with a P_3 type oscillation. The value of η is 0.0338, but the amplitude is so small (23.66 times smaller than in Fig. 1b) that the frequency index is now $\nu = 2.55$. The overall trend of the excitation curve is again in approximate agreement with the trend of the wall formula (the dashed line). The jagged appearance of the curve may be due to the limited statistics of the numerical calculations. (The relative excitation energies are some 30 times smaller than in Fig. 1b, never exceeding 0.8%.) Figure 4a illustrates the opposite extreme of very large excitations, obtained by oscillating in the P_6 mode with $\eta = 0.1$, 0.2 and 0.3 and $\alpha = 0.2$. For $\eta = 0.1$ the relative excitation reaches almost 50% at the end of 5 cycles but the excitation curve still follows closely the wall formula. But for $\eta = 0.3$ the energy of the gas is almost tripled at the end of 5 cycles and exceeds considerably Eq. (5). This discrepancy is qualitatively understandable, since the gas has been heated up to such an extent that the average particle speed $\bar{v}$ must have gone up considerably and the rate of dissipation, as predicted by the wall formula (proportional to $\bar{v}$), would also have increased. An analysis of this problem in the Appendix leads to a generalization of Eq. (5), meant to be valid approximately for arbitrarily long times leading to large excitations. According to this formula the excitation, averaged over the sinusoidal modulations, should be given by

$$\frac{E - E_o}{E_o} \approx \tau + \frac{1}{5}\tau^2 \quad , \tag{11}$$

where

$$\tau = \frac{3}{4}\alpha\eta\ \omega t \quad . \tag{12}$$

This prediction is plotted as the dotted line in Fig. 4a.

Figure 4b shows an aperiodic fission-like deformation of an initially spherical container. Its shape was specified by the volume-conserving equation

$$R(\theta,t) = R_o\left[1 + \alpha P_2\,(\cos\theta)\right]\Big/\left(1 + \frac{3}{5}\alpha^2 + \frac{2}{35}\alpha^3\right)^{1/3} \quad , \tag{13}$$

where $\alpha = \eta v t/R_o$, so that the initial tip speed $\dot{R}(o,o)$, in units of v, is again given by the adiabaticity parameter η. For small α the deformation is approximately spheroidal, but later the shape develops an equatorial neck, whose radius vanishes for $\alpha = 2$, resulting in two somewhat deformed fragment containers in contact. Figure 4b shows that, for relatively small values of η, the process consists of an approximately elastic stage, up to $\alpha \approx 0.3$, where the deformation energy is approximately independent of η. This is followed by a dissipative stage for $\alpha \gtrsim 0.3$, where the excitation energy increases monotonically with the speed of the deformation. Thus, apart from the case $\eta = 0.1$, one might describe the response of the independent-particle gas to a fission-like deformation as that of a piece of rubber, which then melts into a viscous fluid.

3. Oscillations in a fixed container.

Figures 1–4 were studies of the dynamical response of a gas of independent particles in a container whose time-dependence was externally imposed. By contrast, figures 5 and 6 are examples of the dynamical behaviour of a gas in a *fixed* container, the gas executing oscillations analogous to the nuclear giant dipole mode. In Fig. 5a the classical gas with its standard velocity distribution inside a sphere of radius v was started off with an overall speed equal to 0.1v in the z-direction (i.e., the sphere in velocity space was centered a distance 0.1v away from the origin).

The position of the center of mass of the gas (in configuration space) was followed numerically as a function of time for 40 time units R_o/v. The gas is seen to slosh back and forth with an amplitude of some 6%, which is damped to about 2% after three oscillations, whose period is about 5.5 R/v. It is of interest to compare these oscillations with the predicted acoustic dipole mode analogous to the so-called Steinwedel-Jensen hydrodynamical mode underlying an idealized interpretation of the giant dipole resonance in nuclei. The frequency ω of the lowest acoustic dipole mode of a fluid with mass density ρ confined in a spherical cavity of radius R may be written as (Ref. 32)

$$\omega = kc \ , \tag{14}$$

where kR is the first zero, a = 2.081576, of the derivative of the Bessel function j_1 and c is the speed of sound in the fluid in question, given by the square root of the derivative of the pressure with respect to ρ, evaluated at the undisturbed density ρ_o. Thus

$$\omega = \frac{a}{R}\sqrt{(dp/d\rho)_{\rho_o}} \ . \tag{15}$$

In the case of our ideal gas the pressure is given by

$$p = -\frac{d\,(\text{energy})}{d\,(\text{volume})} = -\frac{d\,(\text{energy per particle})}{d\,(\text{volume per particle})}$$

$$= -\frac{d\,(\text{energy per particle})}{d\,(\text{inverse number density})}$$

$$= -\frac{de}{d\,(m/\rho)} = \rho^2 \frac{d\,(e/m)}{d\rho} \ , \tag{16}$$

where e is the energy per particle and m is the particle mass. For an ideal gas

$$\frac{e}{e_o} = \left(\frac{\rho}{\rho_o}\right)^{2/3} \ , \tag{17}$$

where the suffix zero refers to the undisturbed gas. It follows that

$$p = \frac{2}{3}\frac{e_o/m}{\rho_o^{2/3}}\rho^{5/3} \quad , \tag{18}$$

and

$$\left(\frac{dp}{d\rho}\right)_{\rho_o} = \frac{10}{9}(e_o/m) = \frac{1}{3}v^2 \quad , \tag{19}$$

since $$e_o = \frac{3}{5}\left(\frac{1}{2}m\,v^2\right) \quad .$$

The formula for the frequency ω is now

$$\omega = \frac{a}{\sqrt{3}}(v/R) \quad . \tag{20}$$

An alternative way of arriving at this result is to start with the conventional nuclear formula for the Steinwedel-Jensen mode (Ref. 33), written in the form

$$\omega = \frac{a}{R}\sqrt{\frac{2J}{m}} \quad , \tag{21}$$

where J is the nuclear symmetry energy coefficient, and applying it to the case where this coefficient is evaluated for *non-interacting* neutron and proton Fermi gases, whose out of phase oscillations describe the giant dipole mode. With the gases assumed independent, the frequency formula (21) will then apply also to each gas individually. Now the value of J corresponding to this situation is one third the Fermi energy T_F. This is readily verified by writing down the kinetic energies of N non-interacting neutrons and Z protons in a fixed volume, their relative densities being $\left(\frac{N}{A/2}\right)^{2/3}$ and $\left(\frac{Z}{A/2}\right)^{2/3}$, putting $N = \frac{1}{2}A\,(1+I)$, and $Z = \frac{1}{2}A\,(1-I)$, where $A = N + Z$ and $I = (N-Z)/(N+Z)$, and expanding in power of I, thus

$$\begin{aligned} E &= \frac{3}{5}T_F\left(\frac{N}{A/2}\right)^{2/3}N + \frac{3}{5}T_F\left(\frac{Z}{A/2}\right)^{2/3}Z \\ &= \frac{3}{5}T_F(A/2)\left[(1+I)^{5/3} + (1-I)^{5/3}\right] \quad . \\ &= \frac{3}{5}T_F A + \frac{1}{3}T_F A I^2 + \ldots \end{aligned} \tag{22}$$

Hence $J = \frac{1}{3} T_F = \frac{1}{6} mv^2$. Inserting this value in Eq. (21) we again arrive at Eq. (20).

The period T predicted by this expression is

$$T = \frac{2\pi\sqrt{3}}{2.0816} \frac{R}{v} = 5.23 \, (R/v) \quad . \tag{23}$$

This is to be compared with $T \approx 5.5$ (R/v), as read off from Fig. 5a. (One reason for a slight difference might be the fact that in the numerical study underlying Fig. 5a the initial velocity field of the gas did not correspond to a Bessel-function normal mode, so that the resulting oscillation contains an admixture of higher harmonics.) We note that, in contrast to the fair agreement between theory and the numerically observed frequency, the damping of the oscillations is an order of magnitude smaller than would follow from Eq. (7.11) in Ref. (33), based on an application of the wall formula. This might be another illustration of the fact that the wall formula is not meant to apply to situations where the particle dynamics is integrable rather than chaotic.

Figure 5b is also a study of the giant dipole resonance, except that at the initial time the gas had no collective velocity, but instead was distributed non-uniformly in space, with a relative density n_2/n_0 in one half of the spherical container and $(2n_0-n_2)/n_0$ in the other. The induced density oscillations, as measured by the average relative density n_2/n_0, have a period $T \approx 5.6$ R/v. The damping is also similar to that in Fig. 5a.

Figure 6 refers to similar oscillations but for a container in the shape of the non-overlapping portions of two equal overlapping spherical surfaces. In Fig. 6a the area of the window through which the two halves of the container communicate was chosen to be 0.5 of the equatorial cross-section of each sphere and in Fig. 6b this ratio was 0.2. The oscillations are now more strongly damped and, interestingly, the density n_2/n_0 does not equilibrate at $n_2 = n_0$, but settles down to a value in excess of unity. This is readily explained in terms of the special properties of particle trajectories in a spherically symmetric potential. Such trajectories always lie in a fixed plane, and if this plane does not happen to cut the window between the two spheres, the trajectory will never leave the original sphere. The corresponding particle will be 'passive,' i.e., it will not take part in the equilibration process. The fraction of 'active' particles is readily shown to be L/R, where L is

the radius of the window. Thus the unit vector $\check{n}$ which specifies the normal to the trajectory's plane is given by $\check{r}\wedge\check{v}$ where $\check{r}$, $\check{v}$ are the unit vectors associated with the particle's initial position $\vec{r}$ and velocity $\vec{v}$. As $\check{r}$ and $\check{v}$ range uniformly over all possible positions on the unit sphere of orientations, $\check{n}$ will similarly range uniformly over this unit sphere. An active particle is one whose plane of motion (orthogonal to $\check{n}$) intersects the window, which corresponds to a polar hole of diameter 2L/R on the unit sphere. Normals $\check{n}$ to the planes that are required to intersect such a polar hole will then range over an *equatorial belt* of width 2L/R on the unit sphere. The fractional area of the unit sphere belonging to such a belt is L/R, and this is then the fraction of active particles present.

The predicted asymptotic number of particles in sphere 2 will now be given by the number of passive particles in that sphere, plus half the total number of active particles. This leads to the following formula for the asymptotic density $n_2(\infty)$:

$$n_2(\infty) = n_2(o)\left(1-\frac{L}{R}\right)+\frac{1}{2}\left[n_2(o)\frac{L}{R}+n_1(o)\frac{L}{R}\right]$$

$$= n_2(o)-[n_2(o)-1]\frac{L}{R}\ . \qquad (24)$$

The horizontal lines in Fig. 6a,b show these values of $n_2(\infty)$. The numerical results come close to these lines, but the approach seems rather slow. We have not tried to develop a theory of the rate at which the asymptotic behaviour should be attained. This would have to include the discussion of certain periodic or almost periodic orbits, such as triangles, squares, etc., which might continue to miss the window for a long time even though the relevant orbital planes did intersect the window.

4. Poincaré Sections

The elastic or dissipative behaviour of a gas in a slowly deforming container depends on whether the particle trajectories are ordered or chaotic. In order to study the degree of order or chaos of trajectories in such containers, we present a series of Poincaré sections (Ref. 34) illustrating the motions of a sample of particles in statically deformed containers of this type.

These Poincaré sections are generated in our case by imagining the container to be bisected by an equatorial plane and noting the particle's radial distance, ρ, from the symmetry axis and the associated radial velocity, v_ρ, every time the particle crosses this equatorial plane. The result is entered as a point in a plot of v_ρ vs ρ. If the motion is integrable (i.e., if the number of constants of motion is equal to the number of degrees of freedom), the particle's representative point in phase space moves on a torus, the intersection of the Poincaré section with the torus defines a curve, and consecutive points in the (v_ρ, ρ) plane will arrange themselves on such a curve. Conversely, if the motion is chaotic, the points will fill the (v_ρ, ρ) plane in an irregular way.

Figure 1 shows, in the upper part, four Poincaré sections in the case of a spherical container. The first panel refers to the case of planar motions, with zero angular momentum about the z-axis. Ten particles were located at distances from the center equal to $\rho = 0, 0.1, 0.2, \ldots 0.9$ in units of the equatorial radius (equal, in this case, to the radius of the sphere). The particles were then started off with the standard velocity v parallel to the z-axis. The first particle, with initial position $\rho = 0$ and transverse velocity $v_\rho = 0$ keeps bouncing back and forth along the z-diameter of the sphere and (after 150 crossing of the equatorial plane) registers as a single point at the origin of the v_ρ vs ρ plane. The second point, whose ρ-velocity was also zero originally, acquires finite values of v_ρ and traces out a curve in the (v_ρ,ρ) plane.

The other particles trace out similar curves, except for the one started with $\rho = 0.5$. As is readily verified, the corresponding trajectory is a periodic trajectory in the form of a triangle, whose intersections with the equatorial plane occur only at $\rho = 0.5$ and $\rho = 1$, and thus do not trace out a curve.

The second panel in the top row of Fig. 7 corresponds to ten particles started off with a definite angular momentum projection along the z-axis. This was achieved by giving the initial velocity vector (of fixed magnitude v) a tangential component in addition to a component along the z-direction. For each initial ρ the tangential component was chosen so as to give the particle an angular momentum around the z-axis equal to $\sqrt{0.25}$ times the maximum possible (equal to the standard speed v times the radius of the sphere). This requirement sets a lower limit on ρ, equal to

$\sqrt{0.25} = 0.5$. Thus the first particle is started off at $\rho = 0.5$ (in the tangential direction) and the other nine are equally spaced in ρ up to $\rho = 0.95$. The other panels in the first row of Fig. 7 correspond to angular momenta equal to $\sqrt{0.5}$ and $\sqrt{0.75}$ of the maximum possible. The least values of ρ are thus 0.7071 and 0.8660, so that the trajectories in the Poincaré plots are confined to relatively large values of ρ. (The centrifugal force prevents the particles from approaching the z-axis too closely.) All the Poincaré sections correspond to tori in phase space, since motion in a sphere is integrable. This may be contrasted with the second row in Fig. 7 which corresponds to a container deformed according to $1 + \alpha_2 P_2(\cos\theta)$, with $\alpha_2 = 0.5$. In this case the planar motions appear to be chaotic whereas the trajectories with angular momentum equal to $\sqrt{0.25}$ of the maximum possible begin to hint at regularity. The next panel shows a mixture of regular and chaotic behaviour and the ten trajectories in the last panel appear to be regular.

Figure 8 is a similar set of Poincaré plots for a spheroid and for P_2, P_3, P_4, P_5, and P_6 static distortions described by equations like Eq. (1) but without the time dependent factors, and with $\alpha = 0.01$. In Fig. 9, α is equal to 0.05 and in Figs. 10 and 11 α has been increased to 0.1 and 0.2, respectively. Figures 12, 13, 14, and 15 correspond to oblate distortions with $\alpha = -0.01$, -0.05, -0.1, -0.2, and the odd polynomials P_3 and P_5 have been omitted. We note that for the integrable spheroidal distortions the motions are always ordered, as they should be.

For planar motions, order is largely present for sufficiently small deformations, but tends to disappear for larger distortions and larger multipolarities. The survival of tori in phase space for not too large deviations from integrability is a consequence of the Kolmogorov, Arnold, Moser (KAM) theorem (Ref. 34). It is interesting to note that increasing the angular momentum component around the symmetry axis tends to restore order, even for the highest multipolarities. The explanation is surely that a large centrifugal force confines the trajectories to a small region near the container's equator, and since a small portion of such a container can always be approximated by an osculating spheroid, the particle is fooled into believing that it is bouncing inside an only slightly distorted spheroid which, according to the KAM theorem, is expected to exhibit order.

5. Conclusions

The present paper presents numerical evidence for a simple but originally unexpected finding: a gas of independent point particles in a container does not behave at all like a gas. Its response to slow shape changes at fixed volume is sometimes like that of an elastic solid and sometimes like that of a very dissipative fluid. These behaviours are intimately related to whether the dynamics of the individual particles is integrable or chaotic. Even though the studies reported in this paper are entirely at the classical level, the overwhelming effect of the order to chaos transition on the collective dynamics of a classical gas of independent particles can hardly fail to be reflected also in the properties of the system after quantization. The further elucidation of the role of quantization for such systems (Ref. 6) is an outstanding problem, on which we hope to report in due course.

Acknowledgements

J. Blocki and Y.-J. Shi would like to thank the Theory Group of the Lawrence Berkeley Laboratory's Nuclear Science Division for its hospitality.

This work was supported by the Director, Office of Energy Research, Division of Nuclear Physics of the Office of High Energy and Nuclear Physics of the U.S. Department of Energy under Contract No. DE-AC03-76SF00098.

Appendix: Dissipation formula for large excitations

Equation 5 describes the energy of a gas in a periodically oscillating chaotic container. After averaging over the sinusoidal modulations, eq. 5 may be written as

$$\frac{E}{E_o} \equiv y = 1 + \tau \quad , \tag{A1}$$

where τ, equal to $\frac{3}{4}\alpha\eta\omega t$, is a dimensionless measure of time.

The rate of increase of energy implied by the above expression is governed by the wall formula, eq. 4, which contains as a factor the mean speed $\bar{v}$ of the gas particles. As the energy of the gas increases so does $\bar{v}$ and thus also the rate of energy increase predicted by the wall formula. The energy of the gas is proportional to $\overline{v^2}$ and if we could establish a relation between $\bar{v}$ and $\overline{v^2}$ we would be able to write down a differential equation for E valid not only for small excitations (when $\bar{v}$ may be taken to be constant and the result is eq. (A1)).

The relation between $\bar{v}$ and $\overline{v^2}$ depends on the distribution function $f(\vec{v})$ in velocity space (which we shall assume to be isotropic for the chaotic motions under consideration). The simplest situation is one in which, as the gas is heated up, the velocity distribution becomes wider without changing its intrinsic shape. (An example of such behavior is the universal Maxwell-Boltzmann gaussian distribution function whose width is proportional to the energy of the gas.) In that case $\bar{v}$ is obviously proportional to $\sqrt{\overline{v^2}}$, so that the average rate of energy increase would be proportional to the square root of the energy, viz.,

$$\frac{dE}{dt} = K\sqrt{E} \quad , \tag{A2}$$

leading to

$$\sqrt{E} = \sqrt{E_1} + \frac{1}{2}K(t - t_1) \quad , \tag{A3}$$

where E_1 is the value of E at time t_1 and K is a constant. In the dimensionless variables y and τ we may write eq. (A3) as

$$y = y_1 + B\sqrt{y_1}\,(\tau - \tau_1) + \tfrac{1}{4}B^2(\tau - \tau_1)^2 \qquad \text{(A4)}$$

where y_1 is the relative energy when $\tau = \tau_1$, and B is another constant. The above universal linear increase of $\sqrt{E}$ with t might be characteristic of high excitations, where the function f(v) might have reached a universal intrinsic shape, but whether that actually happens is not known.

At the opposite extreme, when f(v) has changed only a little from the step function assumed as the initial velocity distribution of our gas, another universal relation between $\bar{v}$ and $\sqrt{\overline{v^2}}$ may be deduced by using the technique of leptodermous expansions (Ref. 31). Thus assume that f(v) is a slightly diffused step function, like the Fermi function describing a degenerate Fermi gas at low temperature (a distribution qualitatively like a trapezoidal distribution that falls off linearly from one to zero in some small distance c). As we shall show presently, the relation between $\bar{v}$ and $\sqrt{\overline{v^2}}$ is in that case given by

$$\left(\frac{\bar{v}}{\bar{v}_o} - 1\right) = \frac{2}{5}\left(\frac{\overline{v^2}}{\overline{v_o^2}} - 1\right) \quad , \qquad \text{(A5)}$$

where $\bar{v}_o$ and $\overline{v_o^2}$ refer to the values of $\bar{v}$ and $\overline{v^2}$ for the original step function distribution. The above relation is again universal in the sense of being independent of the fall-off profile of f(v). The implied differential equation for E is now

$$\frac{dE}{dt} = k\left(\frac{2}{5}\frac{E}{E_o} + \frac{3}{5}\right) \quad , \qquad \text{(A6)}$$

where k is a constant, whose value is determined by putting $E = E_o$ on the right hand side of eq. (A6), in which case one should recover eq. (A1). Thus $k = \frac{3}{4}E_o\,\alpha\,\eta\omega$. In terms of the dimensionless variables y and τ we now find

$$\frac{dy}{d\tau} = \frac{2}{5}y + \frac{3}{5} \quad . \qquad \text{(A7)}$$

Integrating and expanding in powers of τ we find

$$y = -\frac{3}{2} + \frac{5}{2}\exp\left(\frac{2}{5}\tau\right) = 1 + \tau + \frac{1}{5}\tau^2 + \ldots \qquad \text{(A8)}$$

We may now wish to construct a more generally valid approximate formula for the excitation energy by smoothly joining eqs. (A4) and (A8) at some suitable time τ_1. This determines y_1 and B in eq. (A4) as follows:

$$y_1 = 1 + \tau_1 + \frac{1}{5}\tau_1^2 \quad , \tag{A9}$$

$$B = \left(1 + \frac{2}{5}\tau_1\right) / \sqrt{y_1} \quad . \tag{A10}$$

In order to estimate the time τ_1 at which it would be reasonable to change from the small τ (or small excitation) formula to the large τ (or large excitation) formula, we take as a guide the family of trapezoidal functions f(v), for which the width of the linear surface profile keeps increasing until the trapezoid has become a triangle that begins its linear fall-off already at v = 0. There is at this stage no bulk region left: the distribution has become holodermous (all-surface). The natural further continuation of the sequence of shapes for f(v) is now a holodermous family of triangles of increasing base and decreasing height (ensuring normalization). Making the transition between the leptodermous and holodermous limiting formulae (A8) and (A4) at the moment of the first appearance of the triangle, determines y_1 (and hence τ_1). This is because the relative energy y_1 of a triangular distribution in units of the energy of a step-function distribution containing the same number of particles is readily found to be $y_1 = \frac{4}{3} 2^{1/3} = 1.6799$ leading to $\tau_1 = 0.6064$ from eq. (A9). Inserting these values in eq. (A10) gives the following formulae for the relative energy y:

$$y = 1 + \tau + \frac{1}{5}\tau^2 \quad \text{for} \quad \tau < 0.6064 \quad , \tag{A11}$$

$$y = 1.0109 + 0.9639\,\tau + 0.2298\,\tau^2 \quad \text{for} \quad \tau > 0.6064 \quad . \tag{A12}$$

Comparing these two expressions one realizes that they actually never differ by much, so that the simple expression (A11), formally valid for $\tau << 1$, continues to represent approximately the behavior of y also for large τ. For example, after 5 periods of oscillation in the case illustrated in

Fig. 4a, eq. (A11) gives y = 2.8328 and eq. (A12) gives y = 2.8134. This is a difference of only 0.69%, even though neither y – 1 nor τ (=1.4137) is small at this stage.

The derivation of eq. (A5) proceeds as follows. Consider a leptodermous distribution f(v) qualitatively similar to a Fermi function $[1 + e^{(v-C)/c}]^{-1}$, or to a trapezoidal function

$$f(v) = 1 \quad \text{for} \quad v < C - \tfrac{1}{2}c$$
$$f(v) = 1 - \left[v - \left(C - \tfrac{1}{2}c\right)\right]/c \quad \text{for} \quad C - \tfrac{1}{2}c < v < C + \tfrac{1}{2}c \quad . \tag{A13}$$

Thus we are assuming that f(v) is essentially unity except in a thin surface region, and that the derivative df/dv is a function essentially symmetric with respect to the point v = C. The zeroth moment of f(v), i.e., the normalization integral which we shall write as $\frac{4}{3}\pi R^3$, where R is a constant independent of c, may be written as

$$\tfrac{4}{3}\pi R^3 = \int_0^\infty 4\pi\, v^2\, dv\, f(v) = \tfrac{4}{3}\pi \int_0^\infty dv\, v^3(-f') \quad , \tag{A14}$$

where we have integrated by parts and made use of the vanishing of $v^3 f(v)$ at v = 0 and $v = \infty$. Writing v = C + n we find

$$R^3 = C^3 \int_{-C}^\infty dn \left(1 + \frac{n}{C}\right)^3 (-f') \quad . \tag{A15}$$

Since (–f′) falls off rapidly beyond a distance of the order of the diffuseness parameter c, which is assumed to be small compared to C, we may extend the lower limit of integration to $-\infty$, and order the terms in the integrand according to the small parameter $\varepsilon = c/C$. Thus

$$R^3 = C^5 \int_{-\infty}^\infty dv \left(1 + 3\varepsilon v + 3\varepsilon^2 v^2 + \varepsilon^3 v^3\right)\left(-f'/c\right) \quad ,$$

where v = n/c. Denoting the function (–f′/c) by F(v) and denoting by F_s its s-th moment, viz.

$$F_s = \int_{-\infty}^{\infty} dv\, v^s\, F(v) \ , \tag{A16}$$

we find

$$R^3 = C^3\left(1 + 3\,\varepsilon^2\, F_2\right) \ , \tag{A17}$$

where we have made use of the vanishing of the odd moments due to the assumed symmetry of $F(v)$ with respect to $v = 0$.

Proceeding similarly, the first and second radial moments of $f(v)$, i.e., $\bar{v}$ and $\overline{v^2}$, may be written as

$$\bar{v} = \int_0^{\infty} 4\pi\, v^3\, dv\, f(v) \Big/ \int_0^{\infty} 4\pi\, v^2\, dv\, f(v)$$

$$= \frac{3}{4} C \int_{-\infty}^{\infty} dv (1 + \varepsilon v)^4\, f' \Big/ \int_{-\infty}^{\infty} dv (1 + \varepsilon v)^3\, f'$$

$$= \frac{3}{4} C \left(1 + 6\varepsilon^2 F_2 + \varepsilon^4 F_4\right) \Big/ \left(1 + 3\varepsilon^2 F_2\right) \ ,$$

and

$$\overline{v^2} = \frac{3}{5} C^2 \left(1 + 10\varepsilon^2 F_2 + 5\varepsilon^4 F_4\right) \Big/ \left(1 + 3\varepsilon^2 F_2\right) \ .$$

For $\varepsilon = 0$ we find $\bar{v} = \bar{v}_o = \frac{3}{4} R$ and $\overline{v^2} = \overline{v_o^2} = \frac{3}{5} R^2$, from which, using eq. (A17), it follows that

$$\frac{\bar{v}}{\bar{v}_o} = \left(1 + 6\varepsilon^2 F_2 + \varepsilon^4 F_4\right) \Big/ \left(1 + 3\varepsilon^2 F_2\right)^{4/3} \ , \tag{A18}$$

$$\frac{\overline{v^2}}{\overline{v_o^2}} = \left(1 + 10\varepsilon^2 F_2 + 5\varepsilon^4 F_4\right) \Big/ \left(1 + 3\varepsilon^2 F_2\right)^{5/3} \ . \tag{A19}$$

Expanding to order ε^2 we have

$$\frac{\bar{v}}{v_o} = 1 + 2\varepsilon^2 F_2 + \ldots \tag{A20}$$

$$\frac{\overline{v^2}}{v_o^2} = 1 + 5\varepsilon^2 F_2 + \ldots \ . \tag{A21}$$

Eliminating $\varepsilon^2 F_2$ we find

$$\left(\frac{\bar{v}}{v_o} - 1\right) = \frac{2}{5}\left(\frac{\overline{v^2}}{v_o^2} - 1\right), \quad \text{Q.E.D.} \tag{A22}$$

Equation (A22) is valid when the fourth and higher powers of ε are negligible. In order to estimate the accuracy of this approximation, consider as an example the trapezoidal distribution (A13). We readily find that in this case $F_2 = 1/12$ and $F_4 = 1/80$. We may now calculate $\bar{v}/v_o$ parametrically as a function of $\overline{v^2}/v_o^2$ by means of the exact equations (A18) and (A19), or by means of the lowest-order approximation (A22). We find that in the full range between $\varepsilon = 0$ and $\varepsilon = 2$ (when the trapezoid becomes a triangle) the RMS deviation between the two calculations is 0.06%, with a maximum deviation of 0.17% for $\varepsilon = 2$. Thus the formula $1 + \tau + \frac{1}{5}\tau^2$, based on the leptodermous expansion, turns out miraculously to be almost universal in that it is quite accurate for all values of τ. The dotted curve in Eq. 4a corresponds to this formula. (After this paper was completed a proof that a formula of this type holds exactly for arbitrary times was found. See Refs. 35 and 36.)

References

1. M.C. Gutzwiller, "Chaos in Classical and Quantum Mechanics," Springer-Verlag New York, Inc., 1990.
2. P. Bergé, Y. Pomeau, and C. Vidal, "Order within Chaos," John Wiley & Sons, 1984.
3. "Chaos 87," Proc. Int. Conf. on the Physics of Chaos and Systems far from Equilibrium, M. Duong-van, ed., North-Holland, 1987; Nucl. Phys. **B** (Proc. Suppl.) **2**, 1987.
4. F.M. Izrailev, Phys. Rep. **196**, (1990) 299.
5. O. Bohigas and H. Weidenmüller, Ann. Rev. Nucl. Part. Sci. **38**, (1988) 421.

6. J. Blocki, Y. Boneh, J.R. Nix, J. Randrup, M. Robel, A.J. Sierk, and W.J. Swiatecki, Ann. of Phys. **113**, (1978) 338.
7. J. Randrup and W.J. Swiatecki, Ann. of Phys. **124**, (1980) 193.
8. W.J. Swiatecki, Phys. Scripta **24**, (1981) 113.
9. W.J. Swiatecki, Prog. Particle and Nucl. Phys. **4**, (1980) 383.
10. J.R. Nix and A.J. Sierk, Phys. Rev. **C15**, (1977) 2072.
11. W.J. Swiatecki, Nucl. Phys. **A428**, (1984) 199c.
12. S. Bjørnholm and W.J. Swiatecki, Nucl. Phys. **A391**, (1982) 471.
13. W.J. Swiatecki, Nucl. Phys. **A376**, (1982) 275.
14. M.C. Robel, "Independent particle aspects of nuclear dynamics," Ph.D. thesis, Lawrence Berkeley Laboratory preprint LBL-8181 (1979), unpublished.
15. W.J. Swiatecki, "The nature of nuclear dynamics," Proc. Workshop on Nuclear Dynamics, 22-26 February 1982, Granlibakken, Lawrence Berkeley Laboratory preprints LBL-14138, April 1982, and LBL-14073, April 1982.
16. J.R. Nix and A.J. Sierk, Phys. Rev. **C21**, (1980) 982.
17. J. Carter, C. Brendel, A. Richter, G. Schrieder, H. Feldmeier, W. Bohne, K. Grabisch, H. Lehr, and H. Morgenstern, Z. Phys. **A313**, (1983) 57.
18. G. Fai, Nucl. Phys. **A394**, (1983) 323.
19. H. Feldmeier and H. Spangenberger, Nucl. Phys. **A428**, (1984) 223c.
20. W.J. Swiatecki, in "Nuclear and Atomic Physics with the Accelerators of the Nineties," Z. Sujkowski and G. Szeflińska, eds., Adam Hilger, 1991, p. 219.
21. W.J. Swiatecki, Nucl. Phys. **A488**, (1988) 375c.
22. W.J. Swiatecki, in "Semiclassical Descriptions of Atomic and Nuclear Collisions," J. Bang and J. de Boer, eds., Elsevier, 1985, p. 281.
23. J. Blocki, K. Grotowski, R. Planeta, and W.J. Swiatecki, Nucl. Phys. **A445**, (1985) 367.
24. W. Nörenberg, Nucl. Phys. **A428**, (1984) 177c.
25. J. Negele, Rev. Mod. Phys. **54**, (1982) 914.

26. M. Knudsen, "Kinetic Theory of Gases," Methuen (London) and Wiley (New York), 1950.

27. F. Brut, in "Nuclear and Atomic Physics with the Accelerators of the Nineties," Z. Sujkowski and G. Szeflińska, eds., Adam Hilger, 1991, p. 235.

28. R. Arvieu and Y. Ayant, J. of Phys. **A20**, (1987) 397; **A20** (1987) 1115.

29. R. Arvieu, F. Brut, J. Carbonell, and J. Touchard, Phys. Rev. **A35**, (1987) 2389).

30. J. Carbonell, F. Brut, R. Arvieu, and J. Touchard, J. of Phys. **G11**, (1985) 385.

31. R.W. Hasse and W.D. Myers, "Geometrical Relationships of Macroscopic Nuclear Physics," Springer-Verlag, 1988.

32. H. Lamb, "Hydrodynamics," sixth edition, Dover publications, 1945, p. 506.

33. W.D. Myers, W.J. Swiatecki, T. Kodama, L.J. El-Jaick, and E.R. Hilf, Phys. Rev. **C15**, (1977) 2032.

34. A.J. Lichtenberg and M.A. Lieberman, "Regular and Stochastic Motion," Springer-Verlag, 1983.

35. C. Jarzynski, in preparation.

36. C. Jarzynski and W.J. Swiatecki, "A Universal Asymptotic Velocity Distribution for Independent Particles in a Time-Dependent Irregular Container," Lawrence Berkeley Laboratory preprint LBL-31771, January 9, 1992, to be published.

Figure Captions

Fig. 1. The relative excitation energy of a gas of point particles in a container oscillating fairly slowly with amplitude $\alpha = 0.2$ and adiabaticity index $\eta = 0.04$ around the spherical shape according to Legendre polynomial deformations P_2, P_3, P_4, P_5, and P_6. In (b) the prediction of the wall formula would be indistinguishable from the curve P_5; in (a) the average trend of the wall formula is shown by the dashed line.

Fig. 2. This is like Fig. 1 but the oscillations are spheroidal. In (a) the frequency of oscillation is such that the maximum tip speed of the spheroid, as indicated by the adiabaticity index η, is 0.01, 0.02 and 0.03 times the speed of the fastest particle of the gas. In (b) the frequency has been increased tenfold.

Fig. 3. In (a) the oscillation is a P_2 mode, with amplitude $\alpha = 0.1$ and adiabaticity index $\eta = 0.1414$. In (b) the oscillation is a P_3 mode, with $\eta = 0.0338$ and $\alpha = 0.00845$. The dashed line refers to the trend of the wall formula.

Fig. 4. In (a) the oscillation is in a P_6 mode with $\alpha = 0.2$ and with $\eta = 0.1$ and 0.3. For $\eta = 0.3$ the wall formula prediction is shown by the dashed line and the generalized formula $\tau + \frac{1}{5}\tau^2$ is indicated by the dots. In (b) the spherical container is deformed in a fission-like mode with radius vector proportional to $1 + \alpha P_2$. The rate of change of α is constant, and is such that at the beginning of the motion the tip speed is 0.001, 0.01, 0.02, 0.03 and 0.1 times the speed of the fastest gas particle.

Fig. 5. In (a) the gas inside a spherical container was given an overall velocity along the z-axis equal to 0.1 of the speed of the fastest particle. The position of the center of mass of the gas, in units of R_o, is followed in time as the gas sloshes back and forth in a Steinwedel-Jensen acoustic mode. In (b) the gas was started off with a relative density n_2/n_0 equal to 1.2 in one half of the spherical container and n_1/n_o equal to 0.8 in the other. The subsequent oscillations of the relative density n_2/n_0 are followed in time.

Fig. 6. The plot in (a) is like Fig. 5(a), but the container is in the shape of the non-overlapping portions of two equal spheres, whose intersection defines a window with an area equal to half the equatorial area of either sphere. The horizontal line shows the expected asymptotic value of n_2/n_0 after allowing for the presence of 'passive' particles whose planar trajectories do not intersect the window. In (b) the relative window area has been reduced to 0.2.

Fig. 7. Poincaré sections for ten trajectories in a sphere (upper row) and in a container deformed according to $1 + 0.5\ P_2(\cos\theta)$ (lower row). The first panel in each row refers to planar trajectories, the others to trajectories with angular momentum projections along the axis of symmetry equal to $\sqrt{0.25}$, $\sqrt{0.5}$ and $\sqrt{0.75}$, in units of the maximum possible (see text for details). The position ρ is the radial distance and v_ρ the associated radial velocity of the particle at the moment of crossing the equatorial plane.

Fig. 8. This is like Fig. 7 but for spheroidal and Legendre polynomial deformations specified by $\alpha = 0.01$ (see text).

Fig. 9. This is like Fig. 8 but for $\alpha = 0.05$.

Fig. 10. This is like Fig. 8 but for $\alpha = 0.1$.

Fig. 11. This is like Fig. 8 but for $\alpha = 0.2$.

Fig. 12. This is similar to Fig. 8 but for an oblate deformation $\alpha = -0.01$.

Fig. 13. This is like Fig. 12 but for $\alpha = -0.05$.

Fig. 14. This is like Fig. 12 but for $\alpha = -0.1$.

Fig. 15. This is like Fig. 12 but for $\alpha = -0.2$.

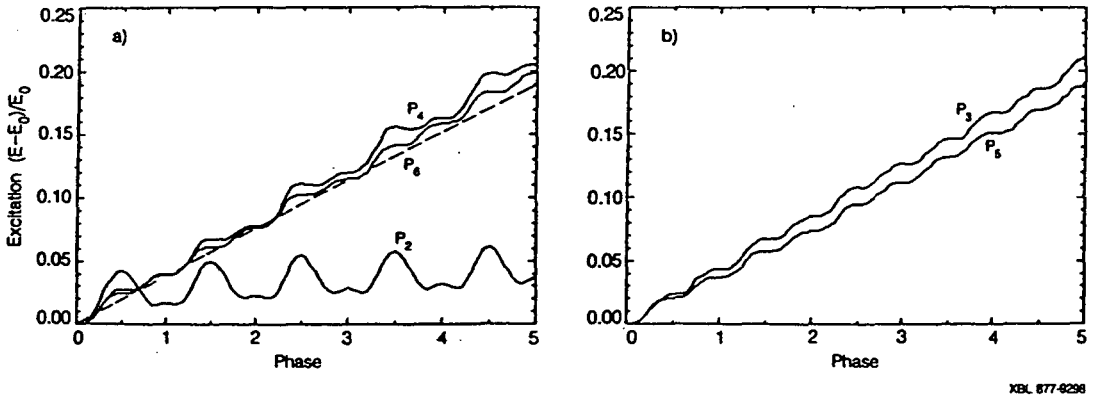

Fig. 1

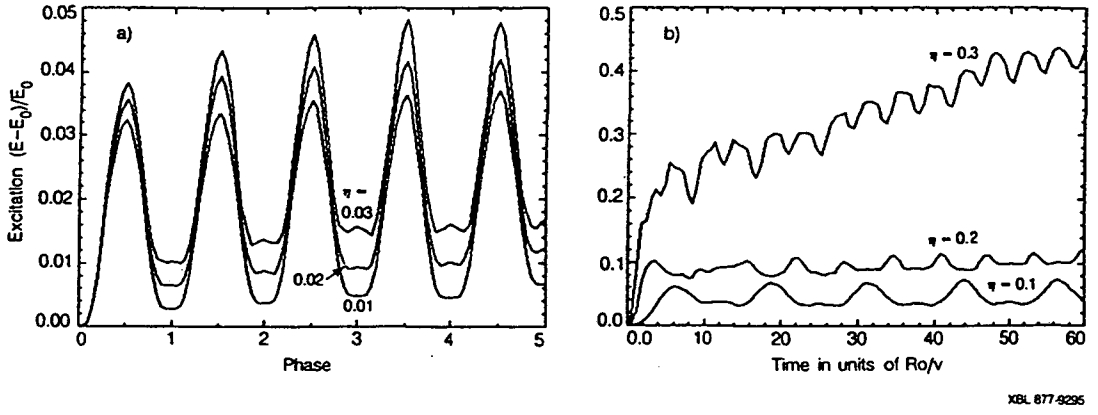
a)
b)
Excitation $(E-E_0)/E_0$
Phase
Time in units of Ro/v
η = 0.03
0.02
0.01
η = 0.3
η = 0.2
η = 0.1
XBL 877-9295

Fig. 2

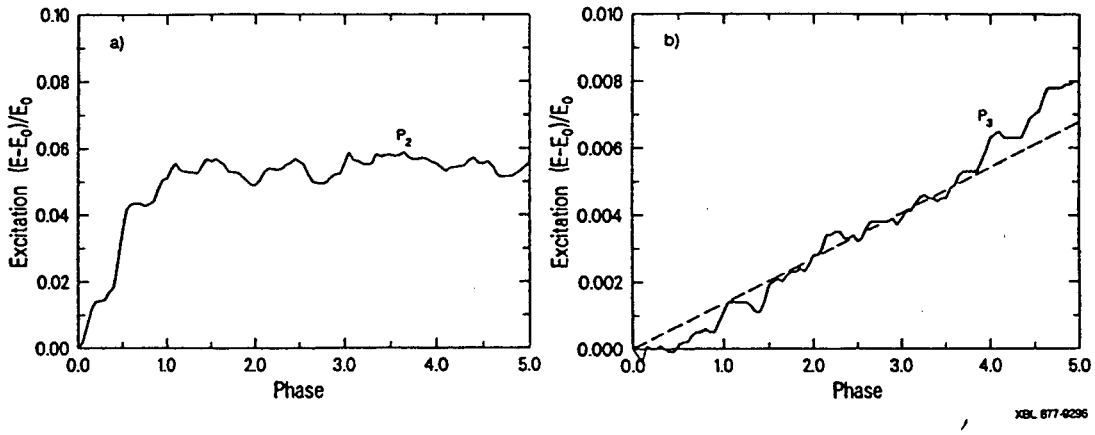
a)
b)
Excitation (E-E0)/E0
Phase
P2
P3
0.10
0.08
0.06
0.04
0.02
0.00
0.010
0.008
0.006
0.004
0.002
0.000
0.0
1.0
2.0
3.0
4.0
5.0
XBL 677-9296

Fig. 3

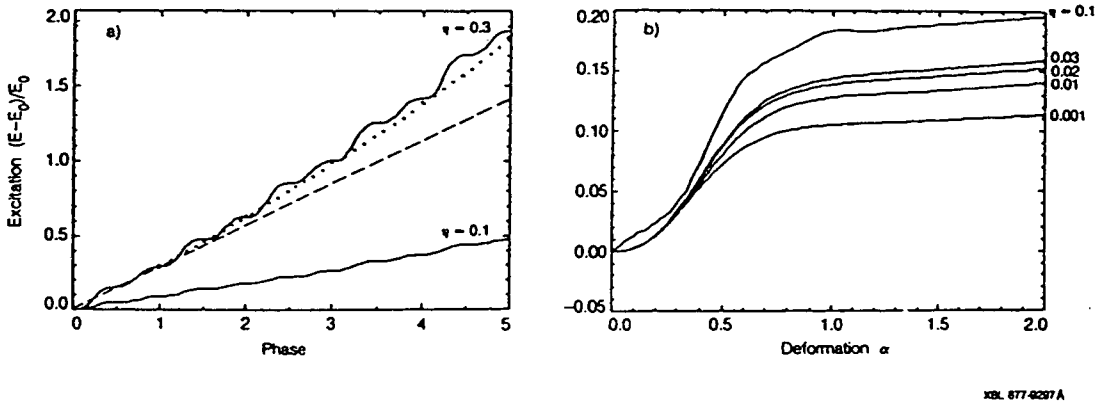
a)
η = 0.3
η = 0.1
Excitation (E−E0)/E0
Phase
b)
η = 0.1
0.03
0.02
0.01
0.001
Deformation α
XBL 877-9297A

Fig. 4

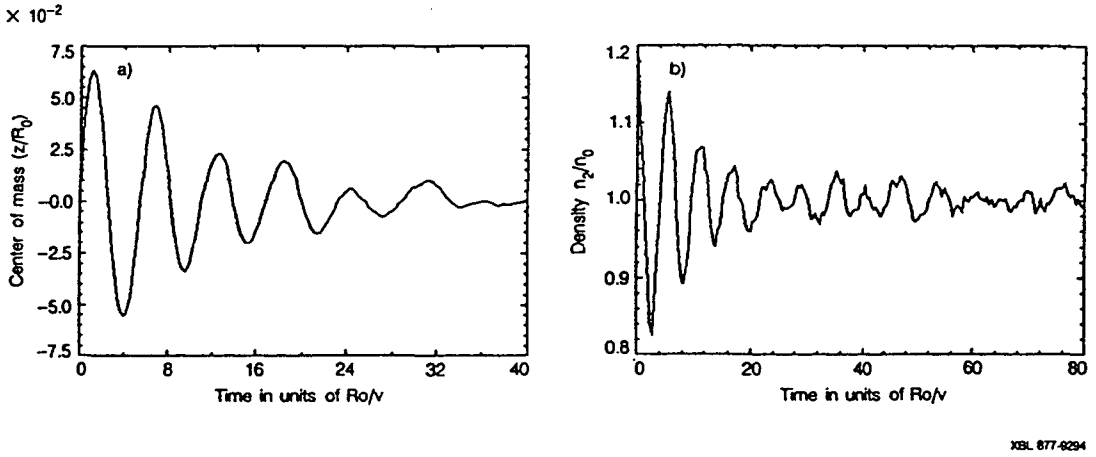
× 10⁻²
a)
Center of mass (z/R0)
7.5
5.0
2.5
-0.0
-2.5
-5.0
-7.5
0
8
16
24
32
40
Time in units of Ro/v
b)
Density n2/n0
1.2
1.1
1.0
0.9
0.8
0
20
40
60
80
Time in units of Ro/v
XBL 877-6294

Fig. 5

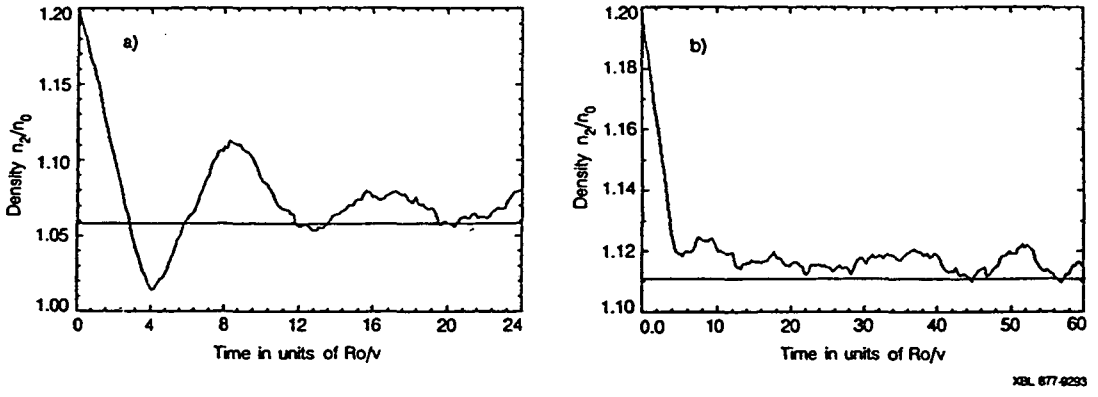
a)
b)
Density n_2/n_0
Time in units of Ro/v
1.20
1.15
1.10
1.05
1.00
0
4
8
12
16
20
24
1.18
1.16
1.14
1.12
1.10
0.0
10
20
30
40
50
60
XBL 877-9293

Fig. 6

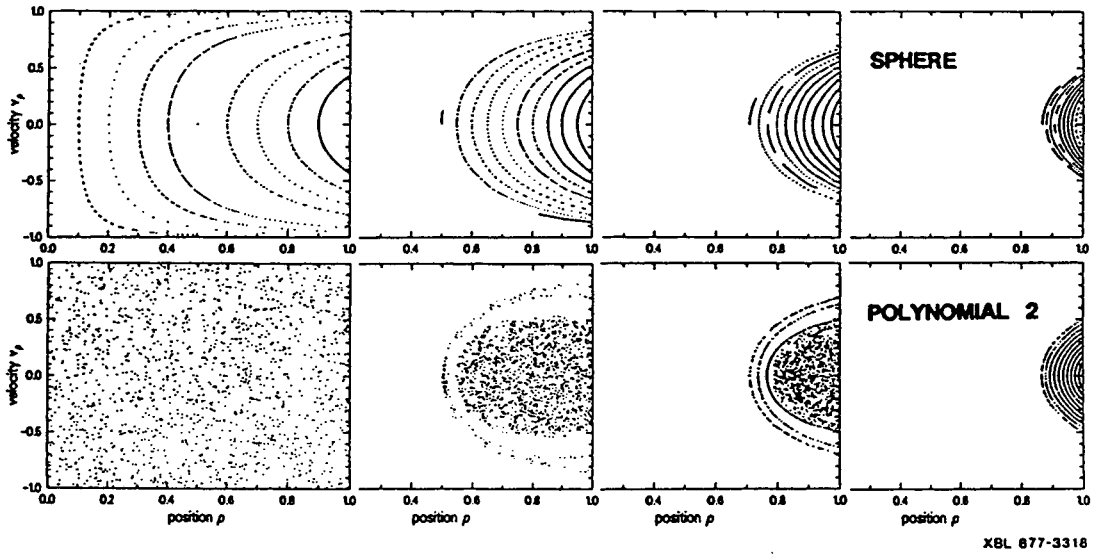
SPHERE
POLYNOMIAL 2
velocity v_ρ
position ρ
XBL 877-3318

Fig. 7

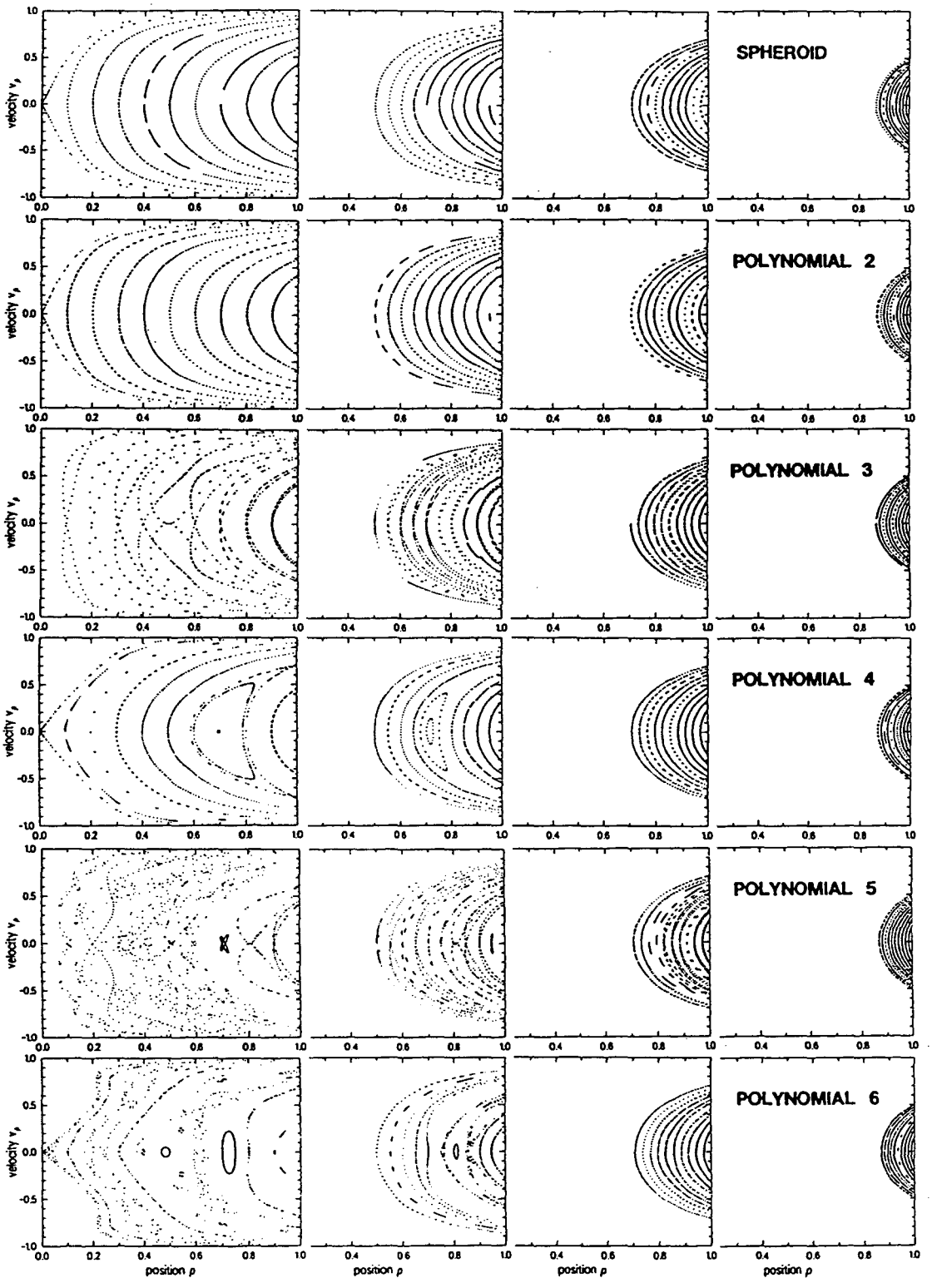
SPHEROID
POLYNOMIAL 2
POLYNOMIAL 3
POLYNOMIAL 4
POLYNOMIAL 5
POLYNOMIAL 6
velocity v_ρ
position ρ
XBL 877-3252

Fig. 8

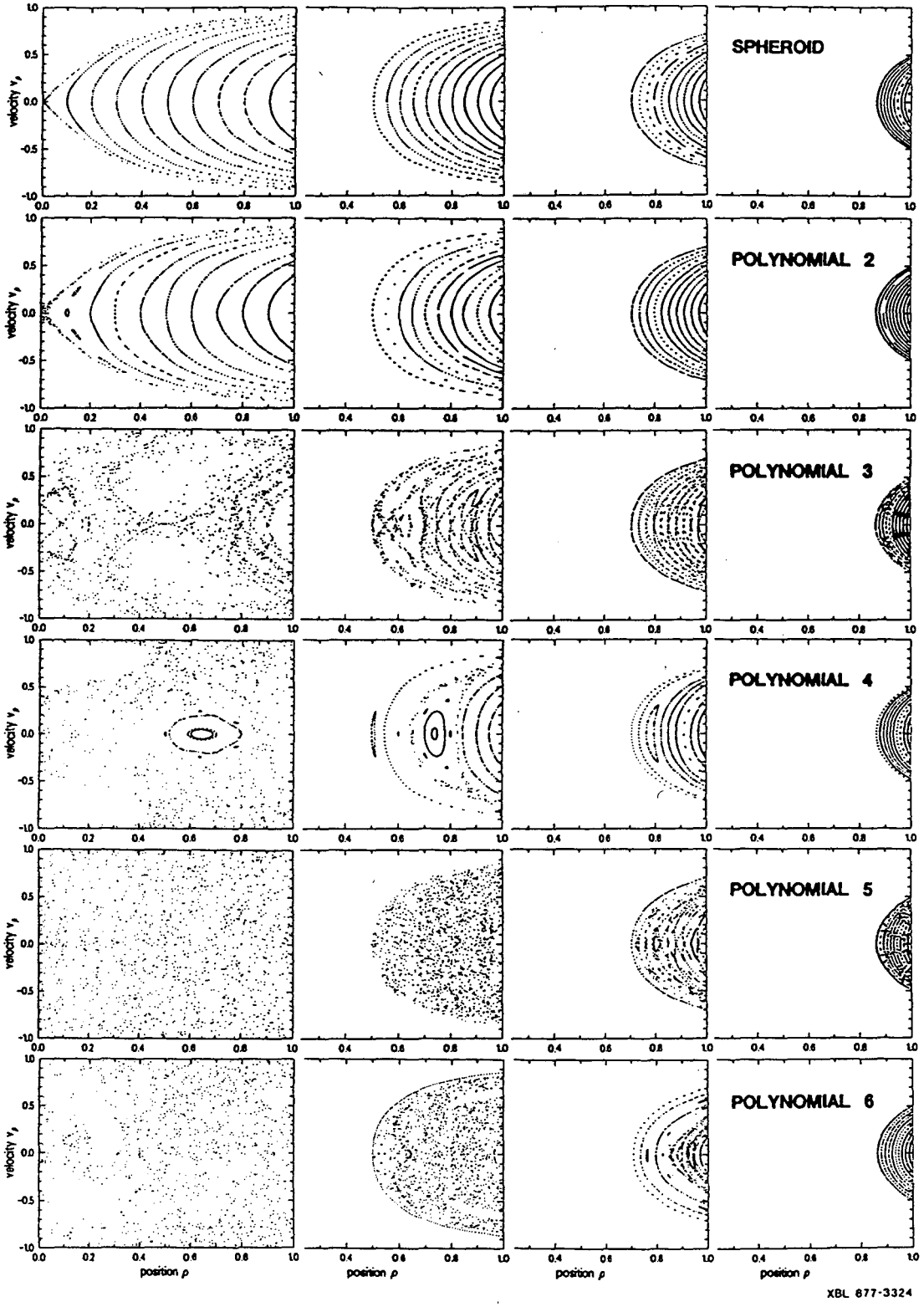
SPHEROID
POLYNOMIAL 2
POLYNOMIAL 3
POLYNOMIAL 4
POLYNOMIAL 5
POLYNOMIAL 6
velocity v_ρ
position ρ
XBL 677-3324

Fig. 9

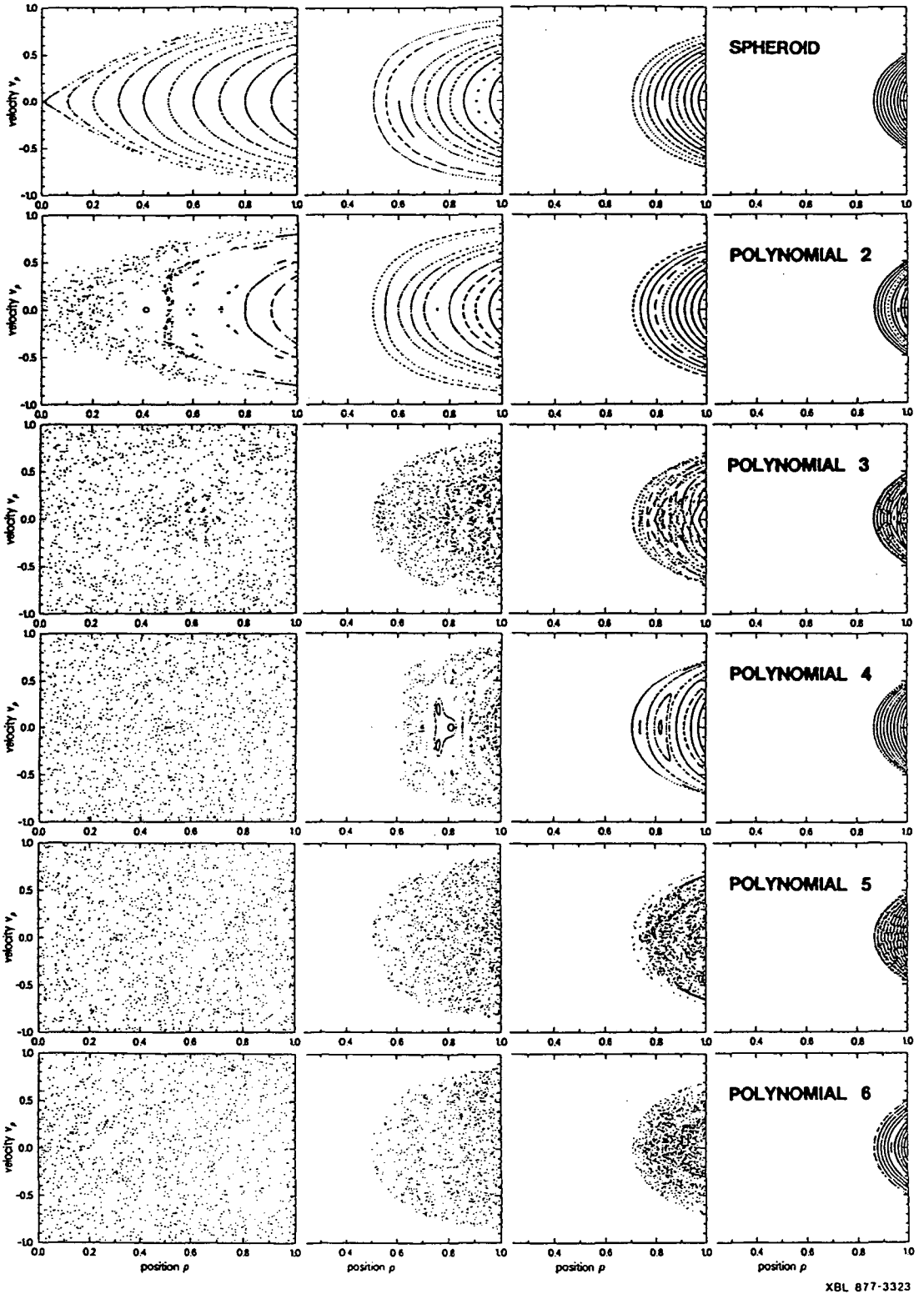
SPHEROID
POLYNOMIAL 2
POLYNOMIAL 3
POLYNOMIAL 4
POLYNOMIAL 5
POLYNOMIAL 6
velocity v_z
position ρ
XBL 877-3323

Fig. 10

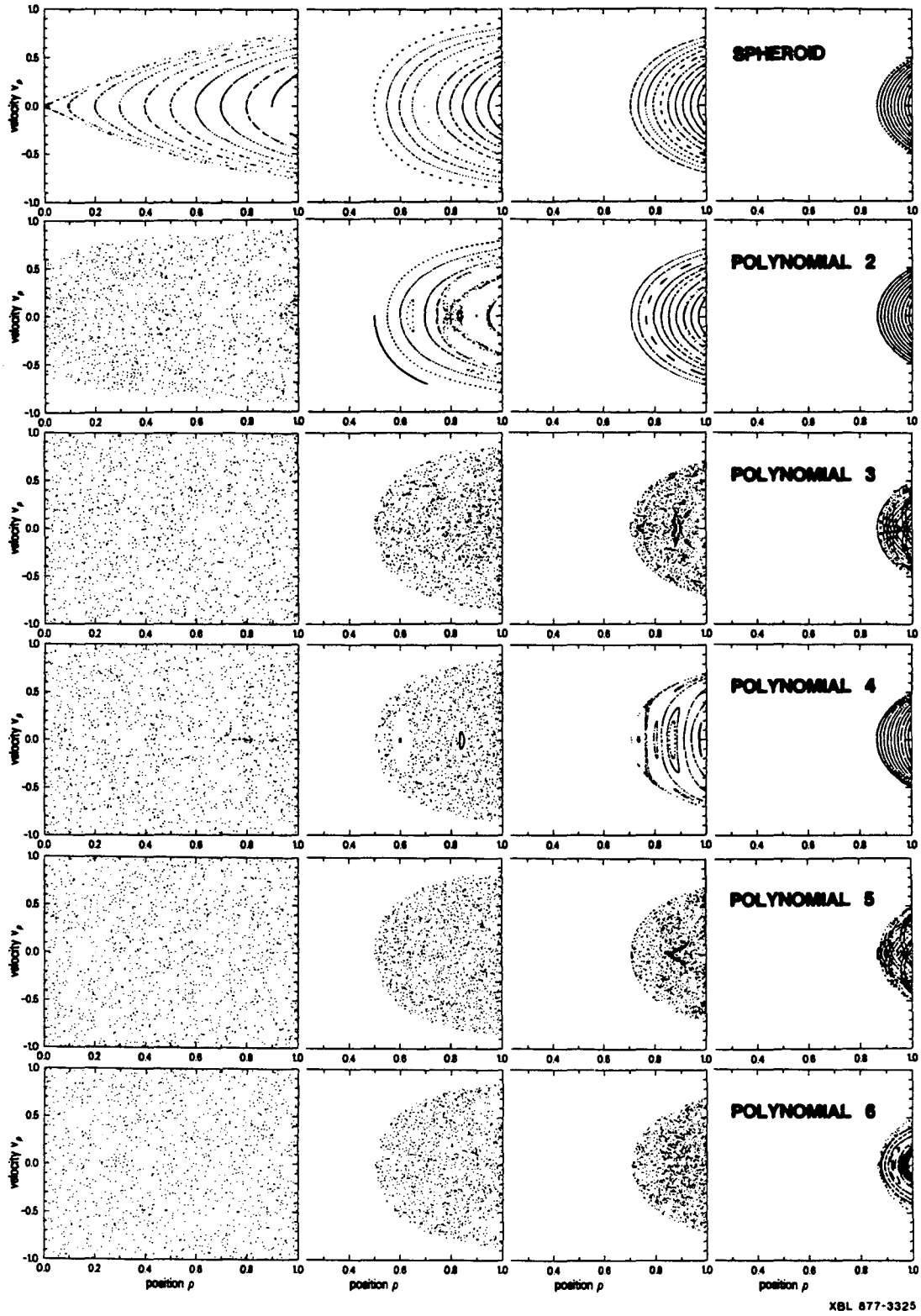
SPHEROID
POLYNOMIAL 2
POLYNOMIAL 3
POLYNOMIAL 4
POLYNOMIAL 5
POLYNOMIAL 6
velocity v_p
position p
XBL 877-3325

Fig. 11

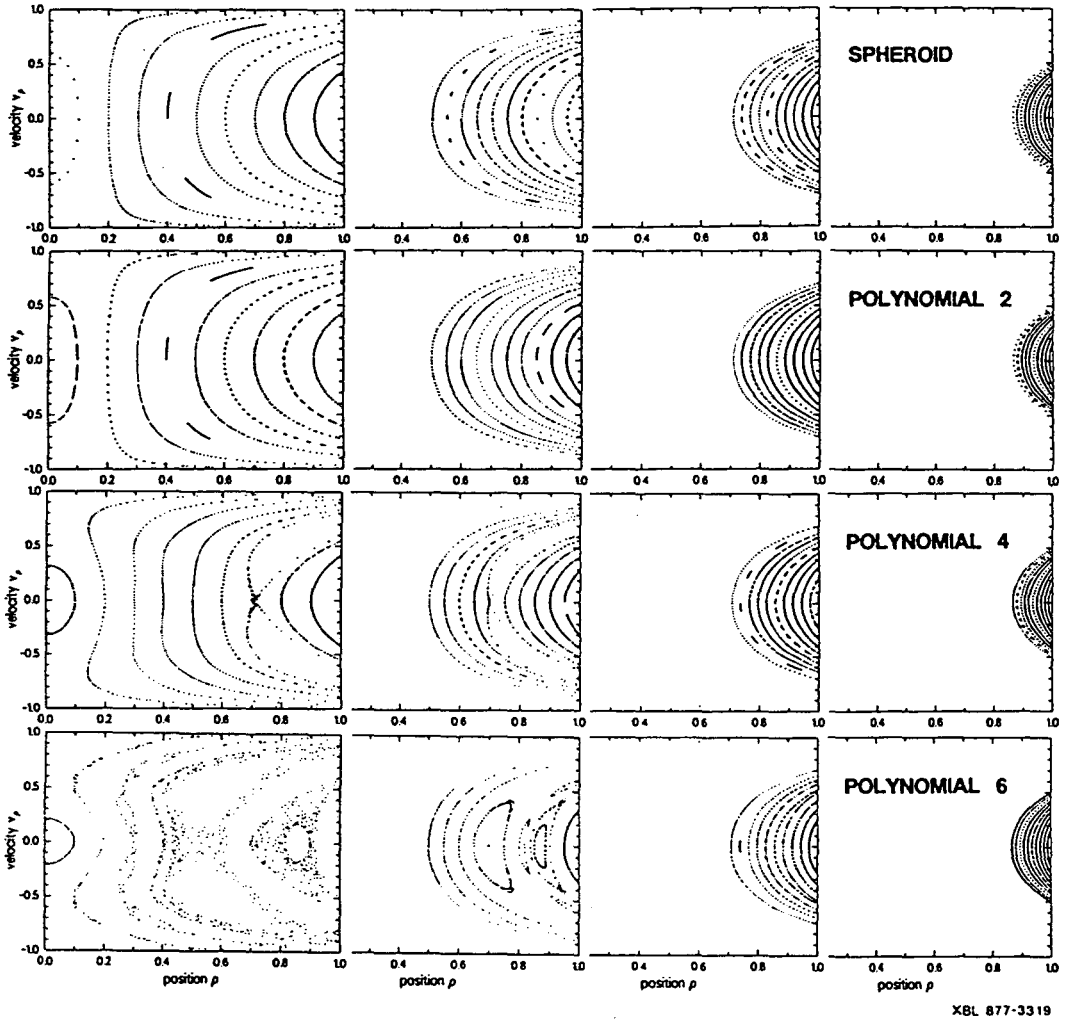
SPHEROID
POLYNOMIAL 2
POLYNOMIAL 4
POLYNOMIAL 6
velocity v_ρ
position ρ
XBL 877-3319

Fig. 12

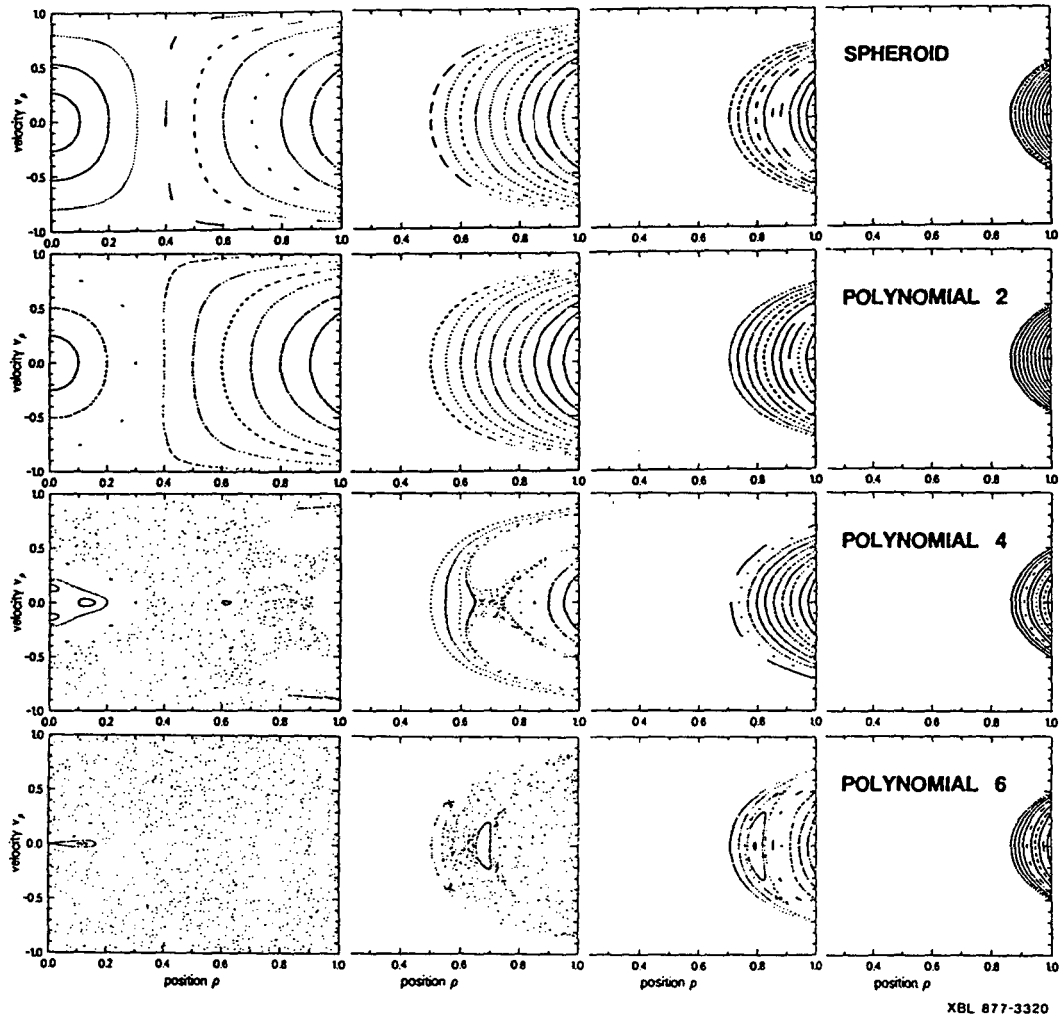
SPHEROID
POLYNOMIAL 2
POLYNOMIAL 4
POLYNOMIAL 6
velocity v_ρ
position ρ
XBL 877-3320

Fig. 13

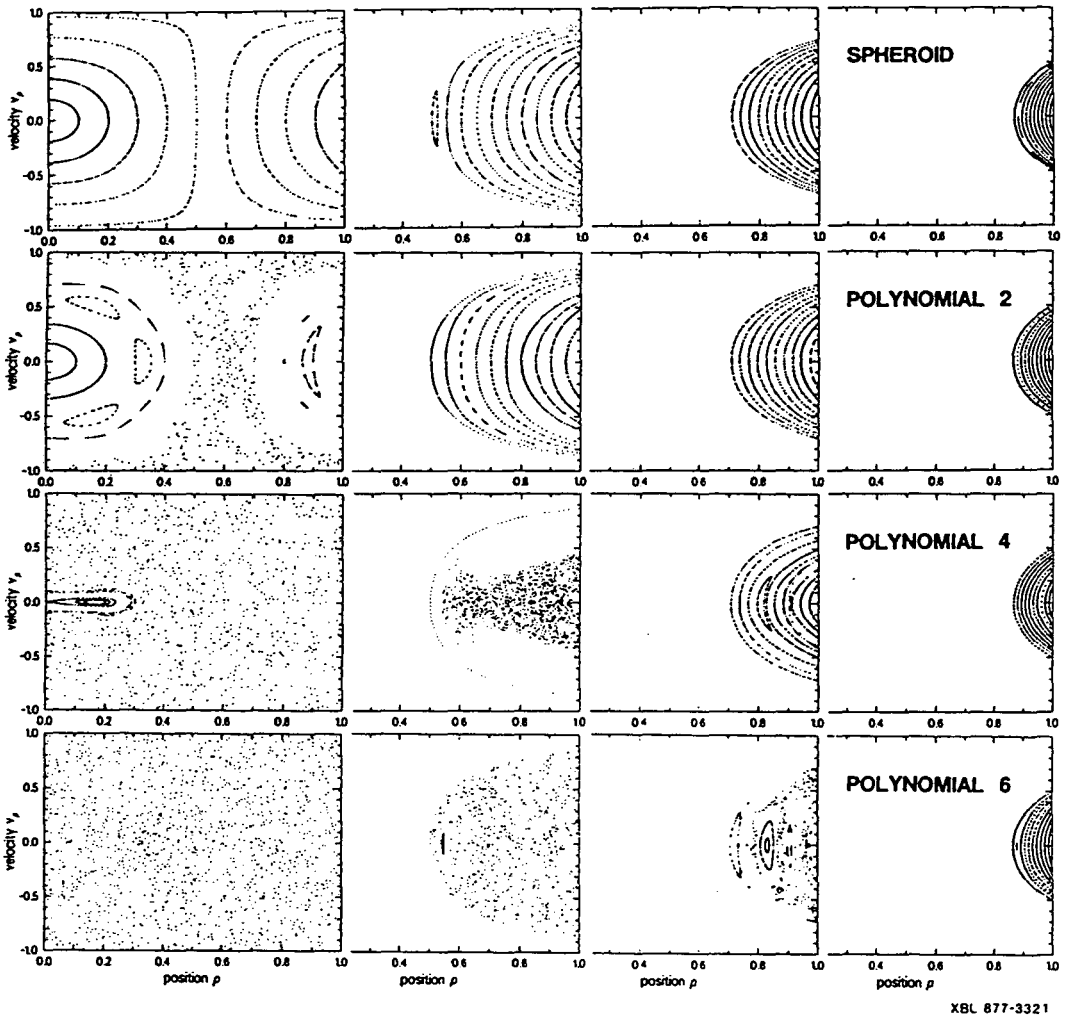
SPHEROID
POLYNOMIAL 2
POLYNOMIAL 4
POLYNOMIAL 6
velocity v_z
position ρ
XBL 877-3321

Fig. 14

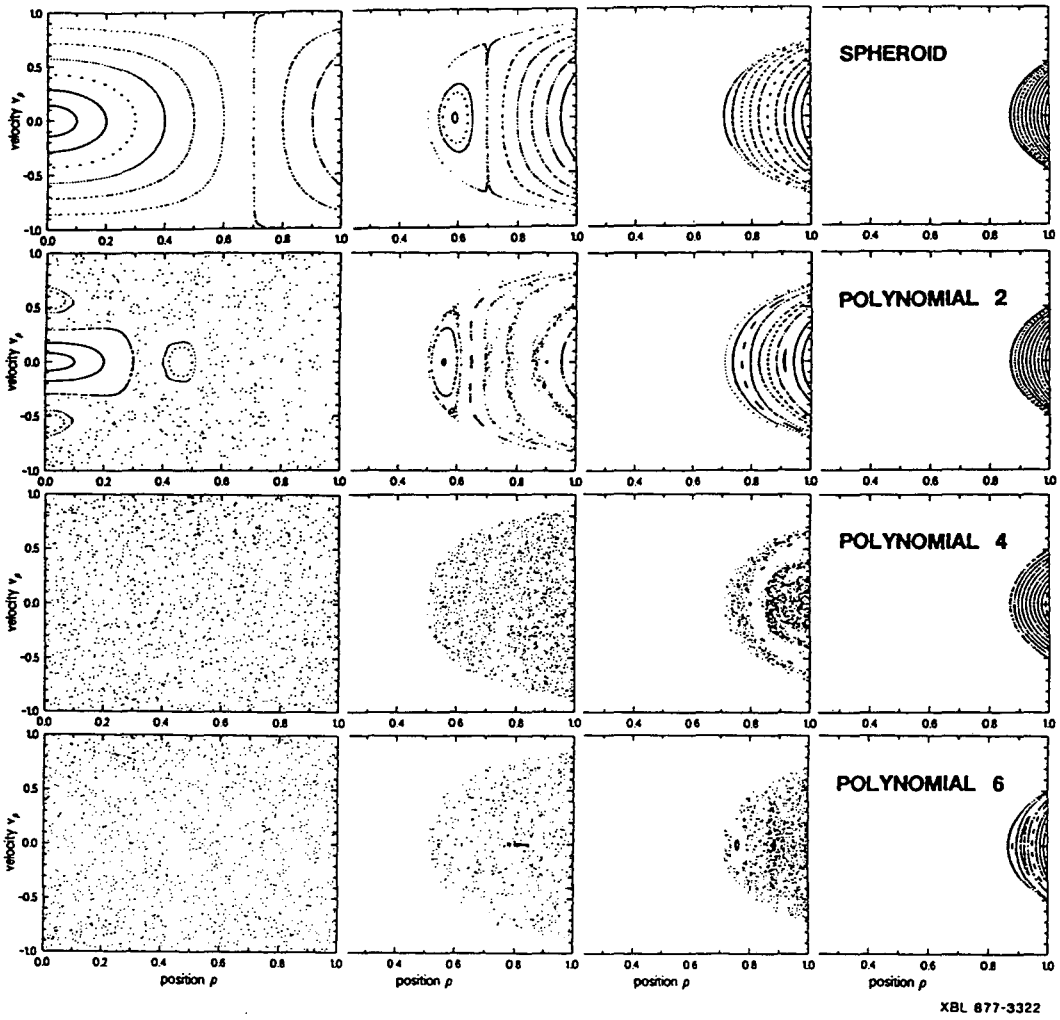
SPHEROID
POLYNOMIAL 2
POLYNOMIAL 4
POLYNOMIAL 6
velocity v_ρ
position ρ
XBL 877-3322

Fig. 15

LAWRENCE BERKELEY LABORATORY
UNIVERSITY OF CALIFORNIA
TECHNICAL INFORMATION DEPARTMENT
BERKELEY, CALIFORNIA 94720